STATE OF THE CLIMATE IN 2015

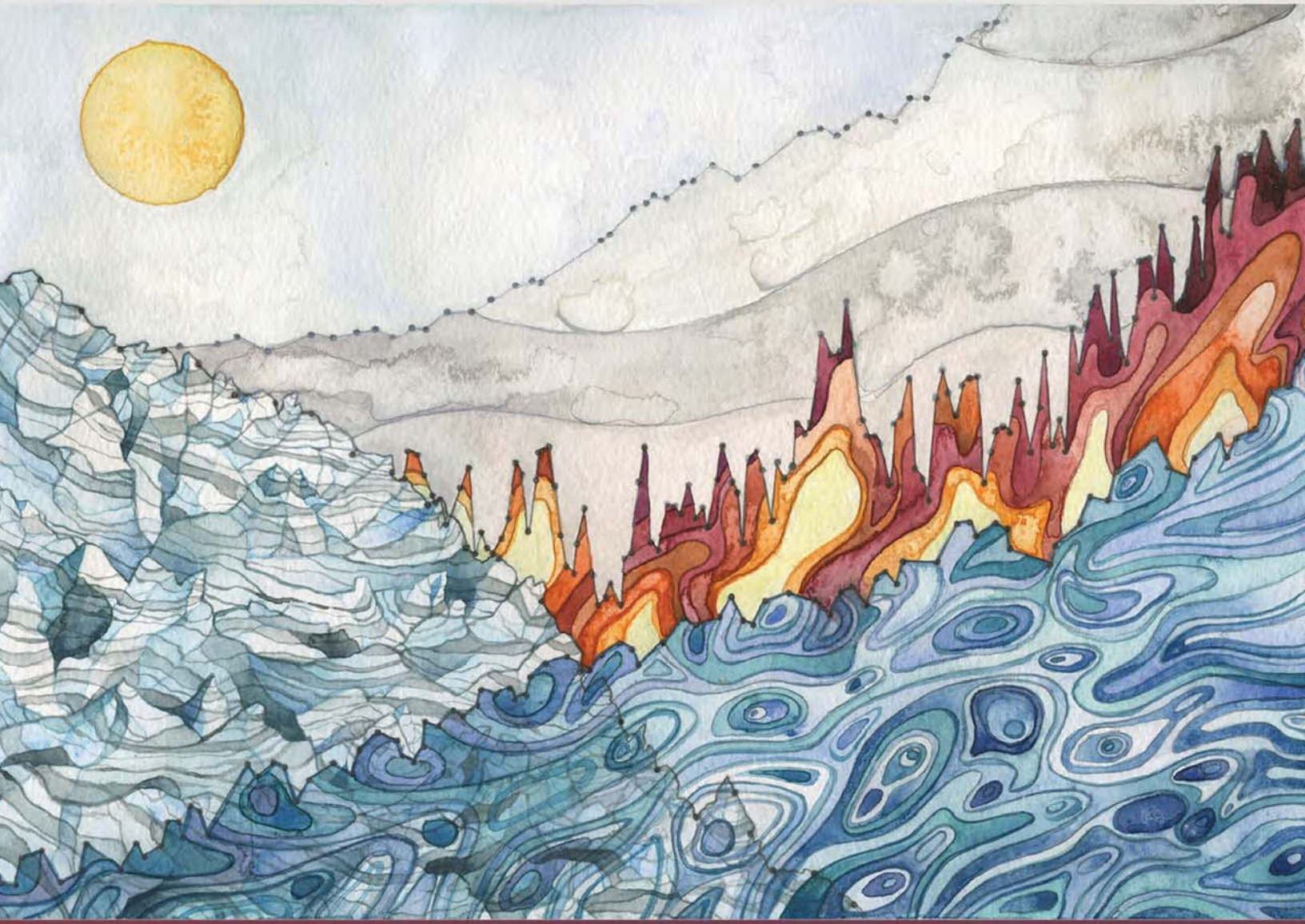

Special Supplement to the
Bulletin of the American Meteorological Society
Vol. 97, No. 8, August 2016

severed during the storm, and four days after the storm nearly 60% of the nation's inhabited islands remained cut off from the outside world. According to UNESCO, 268 million U.S. dollars was required for total recovery and rehabilitation of Vanuatu.

The storm's winds gradually slowed afterwards as Pam tracked west of the Tafea Islands. However, the Fiji Meteorological Service indicated that the TC's pressure dropped farther to 896 hPa on 14 March. As Pam travelled farther south, the storm's eye faded away and Pam's low-level circulation became displaced from its associated thunderstorms, indicating a rapid weakening phase. Later on 15 March, Pam entered a phase of extratropical transition and affected northeast New Zealand and the Chatham Islands with high winds, heavy rain, and rough seas. A state of emergency was declared in the Chatham Islands. At least 15 people lost their lives either directly or indirectly as a result of Pam, with many others injured.

Shortly after Pam was classified, its outer rainbands led to the formation of a tropical low east of Cape York Peninsula, Australia, on 9 March. The Category 1 TC Nathan was named later that day. It slowly executed a cyclonic loop over the next few days, moving across Arnhem Land, Northern Territory, and into Western Australia. See section 4e7 for a detailed timeline of Nathan's development, landfall, decay, and impacts. On 19 March, a tropical disturbance developed about 375 km to the southwest of Apia, Samoa. From 20 to 22 March, the resulting tropical depression produced heavy rain and strong winds over Fiji's Lau Islands. The system moved southward as it was classified as a tropical depression. Early on 22 March, Tropical Cyclone Reuben was named as a Category 1 storm, located about 220 km to the south of Nuku'alofa, Tonga. On 23 March, TC Reuben began extratropical transition.

Tropical Cyclone Solo developed within the monsoon trough on 9 April, about 465 km to the south of Honiara, Solomon Islands. Due to ideal conditions, the system rapidly developed as it moved southward and was named a Category 1 storm. Solo peaked with winds of 54 kt (28 m s^{-1}), making it a Category 2 storm. As Solo turned to the south-southeast from 11 to 12 April, it moved between mainland New Caledonia and the Loyalty Islands. Rainfall totals up to 222 mm were recorded in New Caledonia. Significant damage was reported there, with roads impassable in places and contaminated drinking water in the municipality of Pouébo. Finally, and as noted in section 4e7, Tropical Cyclone Raquel, the last storm of the 2014/15 season, developed as a tropical disturbance about 718 km to the northeast of Honiara, Solomon Islands, on 28 June. Over the next couple of days, the system moved westward into the Australian region, where it was named a TC. Raquel then moved eastward into the South Pacific basin, where it weakened into a tropical depression. On 4 July, the system moved south-westward and impacted the Solomon Islands with high wind gusts and heavy rain.

f. Tropical cyclone heat potential—G. J. Goni, J. A. Knaff, and I.-I. Lin

This section summarizes the previously described tropical cyclone (TC) basins from the standpoint of tropical cyclone heat potential (TCHP) by focusing on vertically integrated upper ocean temperature conditions during the season for each basin with respect to their average values. The TCHP (Goni and Trinanes 2003), defined as the excess heat content contained in the water column between the sea surface and the depth of the 26°C isotherm, has been linked to TC intensity changes (Shay et al. 2000; Goni and Trinanes 2003; Lin et al. 2014). The magnitude of the in situ TCHP was also identified as impacting the maximum potential intensity (MPI) through modulating near-eyewall SSTs (and heat fluxes) occurring when TC winds mechanically mix the underlying ocean (Mainelli et al. 2008; Lin et al. 2013). In general, fields of TCHP show high spatial and temporal variability associated mainly with oceanic mesoscale features, interannual variability (e.g., ENSO), or long-term decadal variability. This variability can be assessed using satellite altimetry observations (Goni et al. 1996; Lin et al. 2008; Goni and Knaff 2009; Pun et al. 2013) or using a combination of altimetry and hydrographic data (Domingues et al. 2015), and has been used to assess meridional heat transport and the overturning circulation in the Atlantic Ocean (Dong et al. 2015).

Globally, the number of tropical cyclones was 10% higher than the previous season; however, in the eastern North Pacific (ENP), the number increased significantly from an already high number in 2014. The 2014 and 2015 ENP hurricane seasons were the most active in recorded history. In the western North Pacific (WNP) basin, the 2015 number was similar to the long-term climatological average. Nevertheless, it is a ~40% increase as compared to the very low occurrence in 2014.

The two following factors best illustrate the overall global TCHP interannual variability within and among the basins: 1) the TCHP anomalies (departures from the 1993–2014 mean values) during the TC seasons in each hemisphere; and 2) differences in TCHP between the 2015 and 2014 seasons.

Most basins exhibited positive TCHP anomalies (Fig. 4.36), except for the WNP and the western portion of the South Pacific basin. The WNP basin experienced a significant reduction in TCHP of ~20%, which is typical of El Niño years (Zheng et al. 2015). The TCHP in the Gulf of Mexico exhibited large positive anomalies due to the intrusion of the Loop Current and a long residence time of Loop Current rings. Despite these positive anomalies, there were no hurricanes in the Gulf of Mexico (just one tropical storm—Bill).

In the ENP basin, the positive TCHP anomalies were consistent with strong El Niño conditions and a continued positive phase of the Pacific decadal oscillation. The combination of these two phenomena is manifest in positive SST anomalies in that region and extending to the date line. Consequently, the TCHP values in this region during the season were even higher than in previous years (Fig. 4.37). As in 2014, positive TCHP and SST anomalies contributed to elevated tropical cyclone activity, with 16 hurricanes in the ENP during 2015 (Fig. 4.36).

The WNP basin also usually exhibits anomalies related to ENSO variability (Lin et al. 2014; Zheng et al. 2015). From the 1990s to 2013, it experienced a long-term decadal surface and subsurface warming associated with prevalent La Niña–like conditions

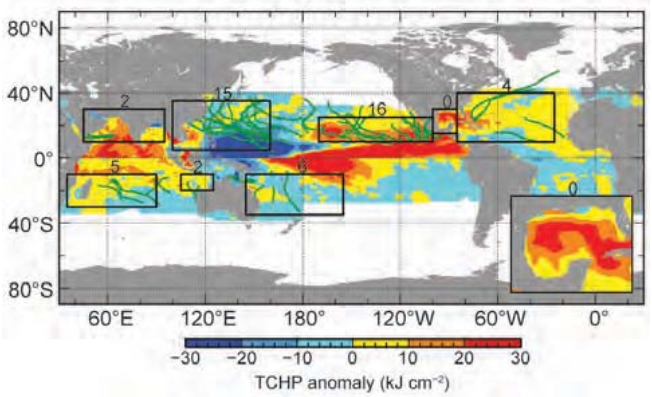

Fig. 4.36. Global anomalies of TCHP corresponding to 2015 computed as described in the text. The boxes indicate the seven regions where TCs occur, from left to right: Southwest Indian, North Indian, West Pacific, Southeast Indian, South Pacific, East Pacific, and North Atlantic (shown as Gulf of Mexico and tropical Atlantic separately). The green lines indicate the trajectories of all tropical cyclones reaching at least Category 1 status (1-min average wind ≥64 kts, 33 m s^{-1}) and above during Nov–Apr 2014/15 in the Southern Hemisphere and Jun–Nov 2015 in the Northern Hemisphere. The numbers above each box correspond to the number of Category 1 and above cyclones that travel within each box. The Gulf of Mexico conditions during Jun–Nov 2015 are shown in the inset in the lower right corner.

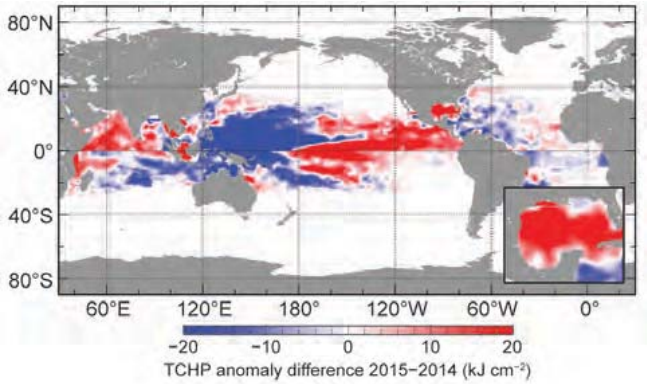

Fig. 4.37. Differences between the TCHP fields in 2015 and 2014 (kJ cm^{-2}).

(Pun et al. 2013; England et al. 2014). However, with the developing El Niño, the warming had stopped. With 2015 being the strongest El Niño event since 1997, the TCHP over the WNP MDR (4°–19°N, 122°E–180°) fell considerably, as characterized by evident negative anomalies (Figs. 4.36, 4.37; Zheng et al. 2015). With the relaxation of the trade winds during El Niño, warm water returning from the western to the eastern Pacific produced a positive anomaly in the ENP while the WNP exhibited a negative anomaly (Figs. 4.36, 4.37; Zheng et al. 2015).

For each basin, the differences in the TCHP values between the most recent cyclone season and the previous season (Fig. 4.37) indicate that the southwest Indian Ocean, the northwest Indian Ocean, and the western portion of the ENP continued to exhibit an increase in TCHP values. TC activity in terms of Category 4 and 5 storms was correspondingly elevated in these basins. The largest changes with respect to the previous seasons occurred in the ENP and WNP basins, with differences greater in magnitude than 20 kJ cm^{-2}. Compared to 2014, the percentage of Category 5 TCs in the WNP was quite low, with only two of 15 TCs (13%) attaining Category 5. In contrast, in 2014, though there were only eight TCs during the TC season, there were three Category 5 TCs or 38%. The evident reduction in TCHP over the WNP may have acted as a damper by increasing the ocean cooling effect on restraining TC intensification (Zheng et al. 2015).

The 2015 season was noteworthy for several reasons with respect to intensification of TCs, including Hurricane Patricia, the strongest Western Hemisphere hurricane ever recorded and Hurricane Joaquin, the most intense TC on record to strike the Bahamas. A summary of the ocean conditions for these and some other selected TCs are as follows.

- Typhoon Koppu (Lando; Fig. 4.38a) was a Category 4 TC that formed east of the Commonwealth

of the Northern Mariana Islands (CNMI) on 10 October. This storm reached its peak intensity on 17 October, with sustained winds of over 100 kt (51 m s^{-1}), and 1-minute sustained winds of approximately 130 kt (67 m s^{-1}). Though it eventually reached Category 4, Koppu did not intensify as rapidly as most intense TCs over the WNP (e.g., Haiyan in 2013; Lin et al. 2014). The negative TCHP may have slowed down its intensification rate (Zheng et al. 2015). However, since the TCHP over the WNP is among the highest globally in a climatological sense, even with reduced TCHP, it is possible for intense TCs to develop (Zheng et al. 2015). During El Niño years, TCs tend to form towards the southeast and closer to the date line. As a result, a TC can travel a longer distance across the ocean during intensification, through over reduced TCHP conditions (Zheng et al. 2015). Koppu made landfall in the north of the Philippines and quickly weakened due to its interaction with land. The cooling of SSTs caused by this typhoon was more evident west of 130°E, in both the surface and upper layer.

- Typhoon Chan-hom (Falcon; Fig. 4.38b) was characterized by its large size and long duration over the ocean. Chan-hom developed on 29 June from an atmospheric system that also developed TC Raquel in the southwest Pacific Ocean. Chan-hom's sustained winds reached values up to 89 kt. (46 m s^{-1}). This typhoon continuously intensified while traveling over warm waters with moderate (> 80 kJ cm^{-2}) TCHP values. A cooling of the surface (–2°C) and the upper layer (40 kJ cm^{-2}) under the track of this typhoon occurred when its intensity reached Category 1.
- Category 5 typhoon Soudelor (Hanna; Fig. 4.38c) was the second-strongest tropical cyclone to develop in the Northern Hemisphere in 2015. Though not as intense as Haiyan in 2013 (Lin et al. 2014), it was as intense as Vongfong in 2014 (Goni et al. 2015). This is in spite of the reduced TCHP in the WNP, associated with the 2015 El Niño year. This drop from the preexisting extremely high TCHP condition (Pun et al. 2013; Lin et al. 2014) was still able to provide favorable conditions for intensification. Soudelor intensified over a very favorable TCHP field of over 120 kJ cm^{-2}, which may have contributed to its ability to attain wind

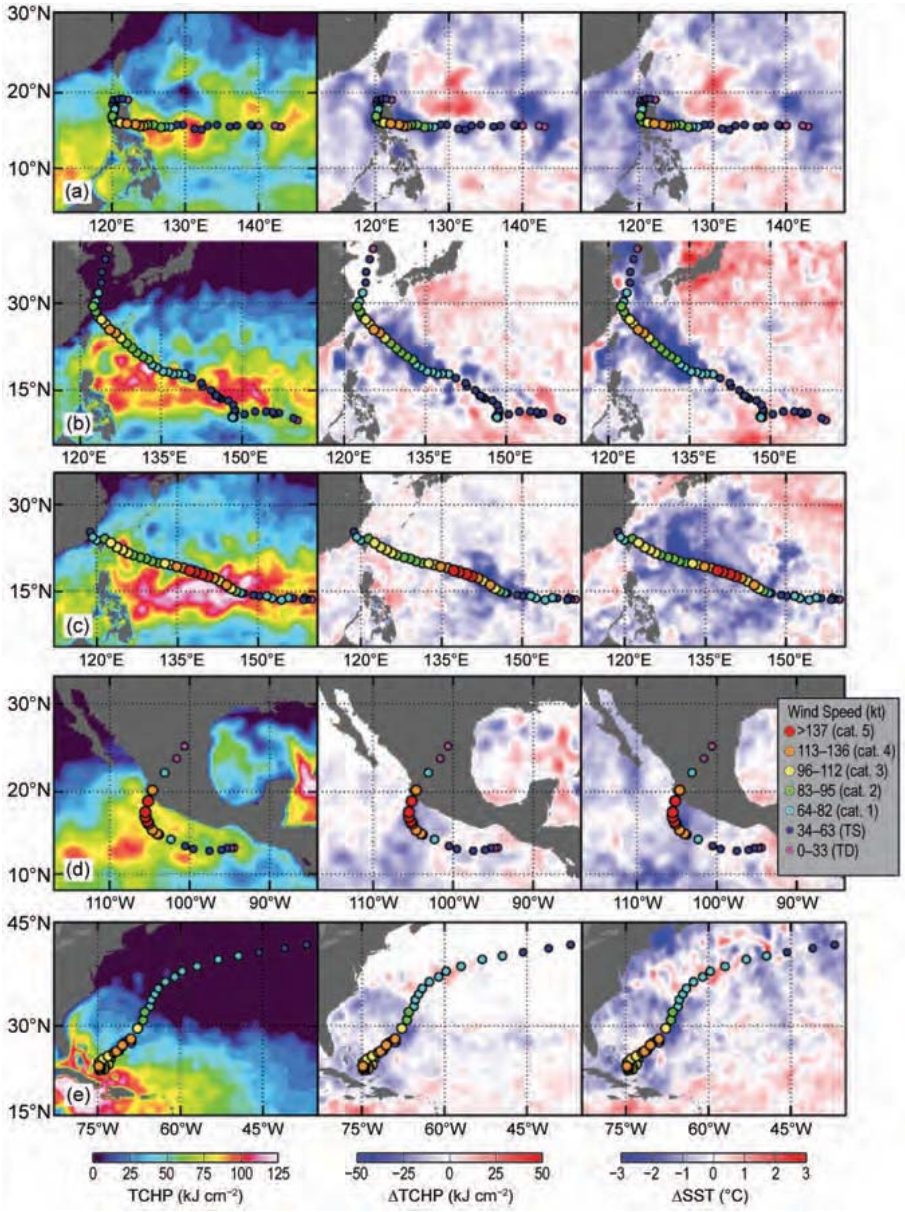

Fig. 4.38. (left) Oceanic TCHP and surface cooling given by the difference between post- and pre-storm values of (center) tropical cyclone heat potential and (right) sea surface temperature, for 2015 Tropical Cyclones (a) Koppu (b) Chan-hom, (c) Soudelor, (d) Patricia, and (e) Joaquin. The TCHP values correspond to two days before each storm reached its maximum intensity value.

speeds of 116 kt (60 m s^{-1}) on 3 August. Its high translation speed (~5–8 m s^{-1}) during intensification helped to reduce the ocean cooling during the TC life cycle, thus supplying more air–sea flux for intensification (Lin et al. 2009). This was the most intense storm to strike Saipan, CNMI, in the last 25 years. Cooling of the surface waters of over 5°C was observed under the full track of this typhoon, while cooling of the upper ocean layers (TCHP) was restricted to between 135° and 150°E.

- Hurricane Patricia (Fig. 4.38d) was the most intense tropical cyclone ever recorded in the Western Hemisphere in terms of barometric pressure, and the strongest ever recorded globally in terms of maximum sustained winds of 185 kt (95 m s^{-1}; Kimberlain et al. 2016). Patricia started as a tropical depression off the coast of Mexico on 20 October, and developed into a Category 5 storm within 66 hours. During its rapid intensification the TCHP values were higher than 80 kJ cm^{-2}.
- Hurricane Joaquin (Fig. 4.38e) was an intense TC that evolved near the Bahamas on 26 September and was one of the strongest storms to affect these islands. Joaquin underwent rapid intensification and became a Category 3 hurricane on 1 October, exhibiting maximum sustained winds of approximately 135 kt (69 m s^{-1}) on 3 October (Berg 2016). The upper ocean conditions were supportive of Atlantic tropical cyclone intensification (Maineli et al. 2008). This rapid intensification occurred during a short travel time over very high TCHP values (> 100 kJ cm^{-2}). The cooling of the ocean waters was evident both in the upper layer and at the surface.

g. Atlantic warm pool—C. Wang

The description and characteristics of the Atlantic warm pool (AWP), including its multidecadal variability, have been previously described (e.g., Wang 2015). Figure 4.39 shows the extension of the AWP time series through 2015 varying on different time scales.

While the AWP in 2015 showed similarities to 2014, there were some key differences. As in 2014, the AWP in 2015 was larger than its climatological mean each month, with the largest AWP occurring in September (Fig. 4.40a). However, the AWP in 2015 started in February and lasted through December, longer than its normal period of May to October, and had an anomalously larger value in November. After starting in February, the AWP appeared in the Gulf of Mexico in June (Fig. 4.40b). By July and August, the AWP was well developed in the Gulf of Mexico and Caribbean Sea and reached eastward into the western

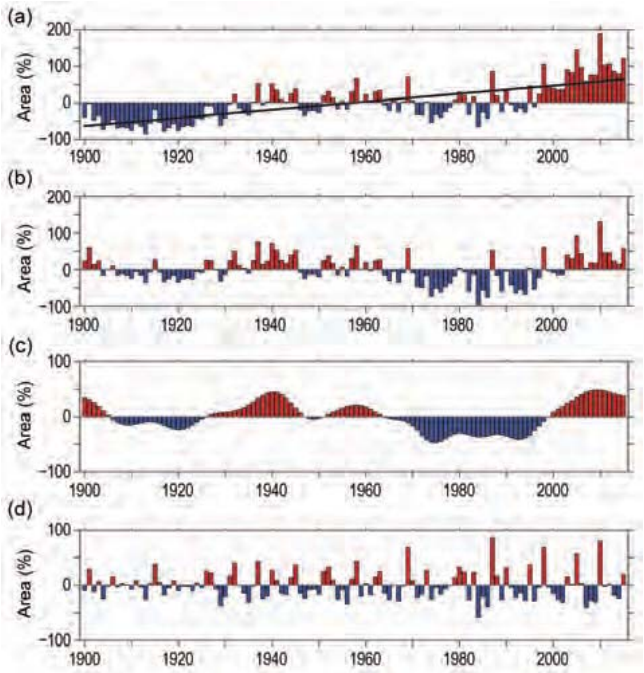

Fig. 4.39. The AWP index for 1900–2015. The AWP area index (%) is calculated as the anomalies of the area of SST warmer than 28.5°C divided by the climatological Jun–Nov AWP area. Shown are the (a) total, (b) detrended (removing the linear trend), (c) multidecadal, and (d) interannual area anomalies. The multidecadal variability is obtained by performing a 7-year running mean to the detrended AWP index. The interannual variability is calculated by subtracting the multidecadal variability from the detrended AWP index. The black straight line in (a) is the linear trend that is fitted to the total area anomaly. The extended reconstructed SST dataset is used.

tropical North Atlantic (Figs. 4.40c,d). By September, the AWP had further expanded southeastward and the 28.5°C isotherm covered nearly the entire tropical North Atlantic (Fig. 4.40e). The AWP started to decay after October when the waters in the Gulf of Mexico began cooling (Fig. 4.40f). In November, the 28.5°C isotherm still covered the Caribbean Sea and part of the western North Atlantic Ocean (Fig. 4.40g).

The effect of the AWP on TC steering flows and tracks has been previously documented (Wang 2015). The TC steering flow anomalies were consistent with those of other observed large AWP years (Wang et al. 2011). The TC steering flow anomalies during the North Atlantic TC season are depicted in Fig. 4.41. With the exception of June and November, the TC steering flow anomalies were unfavorable for TCs making landfall in the United States. From July to October, the TC steering flow anomalies were mostly southward or eastward in the western tropical North Atlantic, and northward and northeastward in the open ocean of the North Atlantic. This distribution